

TinyMyo: a Tiny Foundation Model for Flexible EMG Signal Processing at the Edge

Matteo Fasulo, Giusy Spacone, *Graduate Student Member, IEEE*, Thorir Mar Ingolfsson, *Member, IEEE*, Yawei Li, *Member, IEEE*, Luca Benini, *Fellow, IEEE*, and Andrea Cossetti, *Senior Member, IEEE*

Abstract—Surface electromyography (EMG) is a non-invasive sensing modality used in several domains, including biomechanics, rehabilitation, prosthetic control, and emerging human-machine interaction paradigms. Despite decades of use, significant challenges remain in achieving robust generalization across subjects, recording systems, and acquisition protocols. To tackle these challenges, foundation models (FMs) are gaining traction when targeting end-to-end applications based on EMG signals. Yet, existing EMG FMs remain limited to single downstream tasks and lack deployability on embedded platforms.

In this work, we present TinyMyo, a lightweight FM based on a Transformer encoder architecture. The model is pre-trained in a self-supervised manner on publicly available datasets and achieves high reconstruction fidelity with only 3.6M parameters.

With minimal task-specific head adaptations, the same backbone is used to tackle multiple downstream tasks, leveraging datasets acquired from diverse sensing locations and hardware platforms. We demonstrate generalization across hand gesture classification, hand kinematic regression, speech production and recognition, with performance comparable to or surpassing the state of the art (SoA), and model size below 5M parameters. We achieve SoA results compared to previous FM-based works on the *NinaPro DB5* ($89.4 \pm 0.16\%$), *UCI-EMG* ($97.56 \pm 0.32\%$), and *EPN-612* ($96.74 \pm 0.09\%$) datasets.

We report, to the best of our knowledge, the first deployment of an EMG FM on an ultra-low-power microcontroller (GAP9), achieving an average power envelope of 36.45mW.

By open-sourcing the pre-trained and the downstream task architectures (<https://github.com/pulp-bio/BioFoundation>), we aim to provide a flexible resource that can accelerate future research and serve as a common foundation for the EMG community.

Index Terms—EMG, self-supervised, foundation model, edgeAI, gesture recognition, kinematic regression, speech

I. INTRODUCTION

Electromyography (EMG) measures variations in the electrical activity of muscles during contractions, reflecting the

This work was supported in part by the ETH Future Computing Laboratory (EFCL), financed by a donation from Huawei Technologies, and by a grant from the Swiss National Supercomputing Centre (CSCS) under project ID Ip12 on Alps.

M. Fasulo, G. Spacone, T. M. Ingolfsson, Y. Li, A. Cossetti, and L. Benini are with the Integrated Systems Laboratory of ETH Zürich, Zürich, Switzerland.

L. Benini is also with the Department of Electrical, Electronic and Information Engineering (DEI), University of Bologna, Bologna, Italy.

Correspondence to: Giusy Spacone gspaccone@iis.ee.ethz.ch, Yawei Li li.yawei.ai@gmail.com.

motor-neuron activation patterns [1]. EMG can be acquired using invasive methods (needle EMG), suitable for a detailed characterization of individual motor units, or using non-invasive, surface-based techniques, to capture the global activity of muscle fibres [1], [2].

Surface EMG has found extensive application across a wide range of domains, including biomechanical analysis and rehabilitation [2], human–robot interaction [3], prosthetic control [4], [5], and emerging human–computer interaction interfaces [6]. However, despite decades of widespread use, many important challenges remain.

First, EMG signals are highly affected by noise, motion artifacts, and cross-talk from adjacent muscles [7]. Also, acquisition systems present large variability in terms of number and arrangement of electrodes, sensor geometry, sampling rates, amplification stages, and filtering pipelines [8]. These sources of variability pose challenges to the design of models that can generalize across heterogeneous hardware configurations. In addition, EMG recordings are strongly influenced by both inter-subject and intra-subject variability [9]. Differences in anatomy, subcutaneous fat, electrode placement, skin impedance, and day-to-day physiological or behavioural factors lead to substantial shifts in the EMG distribution, posing an additional challenge to generalization across users or recording sessions [10].

Foundation Models (FM) offer a great promise to address these challenges. Inspired by the success of self-supervised pre-training in vision, language, and speech, as well as by emerging applications in biosignals [11], the core hypothesis is that large-scale datasets can be leveraged to learn high-level, platform and subject-agnostic signal representations. For EMG, such models could provide a unified backbone for many downstream tasks, building upon a robust, device-agnostic feature extraction, improving generalization across devices and subjects. However, progress in FMs of EMG has been limited by the scarcity of large sEMG corpora, and only with recent large-scale datasets (collected from thousands of users) [12] the exploration of generalized FMs of EMG became viable.

In this context, existing EMG FMs present significant limitations. Current models mostly focus on a single task (typically gesture classification) [13], [14]. Furthermore, the size of EMG FMs remains large, and no prior work demonstrated the deployment of an EMG FM on embedded hardware. This motivates the need for efficient FM architectures that meet the memory and computational constraints of embedded devices

[15].

We address these limitations by proposing the following contribution.

- We present **TinyMyo**, a lightweight Transformer-based encoder operating directly on EMG signals in the time domain. TinyMyo is pre-trained using a self-supervised masked-reconstruction framework on publicly available, heterogeneous sEMG datasets, achieving high reconstruction fidelity with only **3.6 million** parameters.
- Unlike previous EMG FMs, which are typically designed around a single downstream task or rely on large, domain-agnostic encoders, TinyMyo **generalizes across heterogeneous sEMG datasets and sensor configurations**. Our architecture follows the general Transformer design adopted in prior EMG works [13], [14], formulated in a *unified EMG* FM able to support a wide range of downstream tasks using the same pretrained backbone. We demonstrate the versatility of the pre-trained encoder through minimal task-specific head adaptations across diverse downstream tasks, including **hand-gesture classification** on the Ninapro DB5 [16], EPN-612 [17], UC Irvine [18] and Meta’s Generic Neuromotor Interface [6] datasets, **hand-kinematic regression** on the Ninapro DB8 [19], and **speech** production and discrimination on the Gaddy Silent Speech Dataset [20]. Our model achieves competitive performances across all downstream tasks, either surpassing SoA or guaranteeing a comparable accuracy with a sub-5M class model size.
- We demonstrate for the first time the **deployment of an EMG FM on an ultra-low-power microcontroller** (GAP9), achieving an average power envelope of 36.45mW.
- We open source the model and weights to enable reproducibility and further research by the community.

II. RELATED WORKS

Several efforts have been made to develop FMs for biosignals, and most of the works focused on electrocardiography (ECG), photoplethysmography (PPG), and electroencephalography (EEG) [10]. In contrast, research dedicated to EMG FMs remains limited.

Turgut et al. [21] introduced OTiS, a foundation model with 45 M parameters pre-trained on a broad collection of modalities, including ECG, temperature, audio, electromechanical signals, EEG, and financial time series. Their work demonstrated the feasibility of handling heterogeneous time-series data, including diverse input types, sampling rates, and channel configurations, within a unified pre-training framework. In the original study, EMG is used exclusively for multi-class muscular disease classification. Subsequent works by Cheng et al. [13], [14] evaluated the same model on hand-gesture classification using the EPN612 [17], NinaPro DB5 [16], NinaPro DB6 [22], and UCI EMG [18] datasets, demonstrating high accuracy across all datasets.

Goswami et al. proposed MOMENT [23], a 350-M parameter FM pre-trained on a wide range of domains and temporal resolutions, including electrical signals, traffic, weather, disease progression, motion capture, simulated data, and ECG

(among biopotentials). In the original work, EMG is not included in the pre-training corpus nor in the downstream evaluations. However, recent studies by Cheng et al. [13], [14] assessed MOMENT on the hand-gesture classification task using the EPN612, NinaPro DB5, NinaPro DB6, and UCI EMG datasets, demonstrating the applicability of MOMENT as an EMG FM.

PhysioWave [13] introduced a modality-specific FM for EMG and ECG. The authors further propose a unified multimodal framework combining these encoders with existing pre-trained EEG models, leveraging a multi-scale wavelet-transformer architecture, using wavelet decomposition to capture time-frequency features at different scales. For the EMG-specific model, the primary downstream task is hand-gesture classification, evaluated on NinaPro DB5, EPN612, and UCI EMG. PhysioWave achieved a performance comparable to Moment and OTiS with a much smaller parameter count (5M for the smaller model).

The same authors proposed WaveFormer [14], a lightweight Transformer model tailored for sEMG-based gesture recognition, with a model size of only 3.1 M parameters. To ensure the extraction of frequency-domain features remains compact, the model integrates a learnable wavelet transform based on multi-level wavelet decomposition and depthwise separable convolutions. Downstream evaluations are conducted on the EPN612, NinaPro DB5, NinaPro DB6, and UCI EMG datasets, further improving the performance over PhysioWave.

More recently, Jiang et al. [24] introduced PhysioOmni, a multi-modal FM designed to handle a wide range of physiological signals such as EEG, ECG, EOG and EMG. For each modality, the authors use the same encoder as in LaBrA-M [25] (5.8M parameters per modality, considering its smallest-Base version). They adopt a decoupled multimodal tokenizer and masked signal modelling to ensure robustness under arbitrary missing modalities during inference. During pre-training, PhysioOmni relies on a fixed set of modalities (EEG, EOG, and EMG), which makes the architecture unsuitable for pre-training when one modality is missing. For downstream evaluation, the authors include 5-class sleep stage classification on the HMC [26] dataset and gait kinematic regression on the FBM [27] dataset.

In this context, existing EMG FMs appear limited by the small number of explored downstream tasks, as well as by the lack of deployability on embedded platforms. TinyMyo is the first EMG FM to cover a broader range of downstream tasks with SoA performance, as will be extensively described in Section IV, while also being deployed on an ultra-low-power MCU.

III. METHODS

Figure 1 shows the TinyMyo framework. In the following sections, we present the strategy adopted for model pre-training (Sect. III-A) and downstream tasks (Sect. III-B).

A. Foundation Model Pre-Training

1) *Tokenization*: TinyMyo adopts a Channel-Independent patching strategy, following methodologies effectively applied

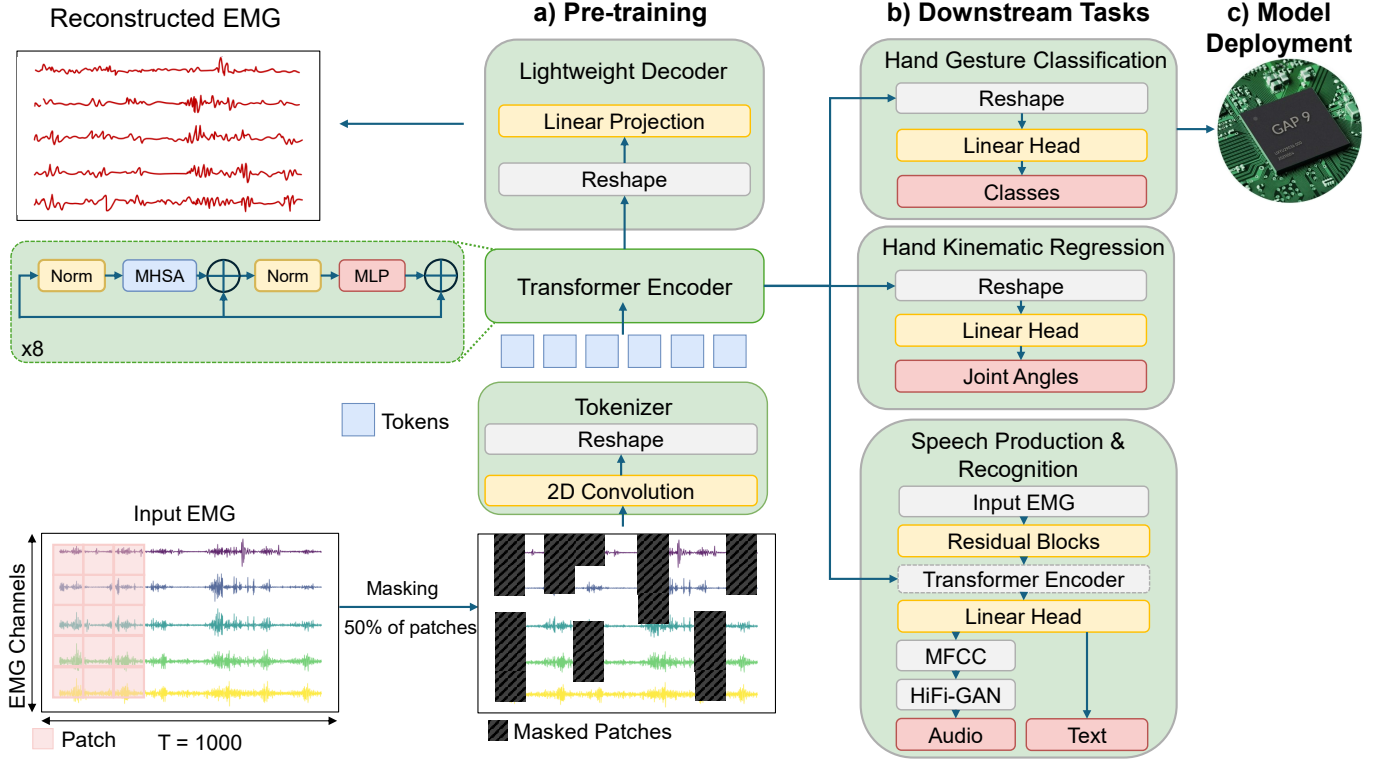


Fig. 1. Overview of the TinyMyo architecture. (a) Pre-training framework: the input signal is first tokenized using a channel-independent patching strategy with random masking, processed by eight bidirectional Transformer Encoder blocks, and reconstructed by a Lightweight Decoder. (b) Downstream architectures: after pre-training, the Decoder is removed and replaced with task-specific heads. For Hand-Gesture Classification and Kinematic Regression, a linear head is used to produce output classes or joint angles. For speech-related tasks, the EMG input is first downsampled through residual convolutional blocks and then passed through the pre-trained Transformer Encoder, followed by a linear head. The output is text for the Speech Recognition task. For the the Speech Production task, a vocoder (HiFi-GAN) is added to produce audio from the predicted MFCC features. (c) Model Deployment: the architecture for the hand-gesture classification task is implemented on the GAP9 microcontroller.

in time-series forecasting [28] and vision [29]. Unlike other recent biosignal (EEG) foundation models that mix spatial information during the tokenization phase via 2D convolutions that span multiple channels (e.g., FEMBA uses a 2×16 kernel [30]) or project them into a unified latent space (e.g., LUNA [31]), we strictly maintain per-channel granularity. This design choice is grounded in the physiological nature of EMG recordings, where each channel corresponds to a distinct anatomical location. By treating the channels independently at the embedding stage (using a $1 \times L$ kernel), the model allows the subsequent transformer layers to learn inter-channel dependencies via attention, a strategy proven effective for biosignal decoding [32].

Formally, let the input EMG waveform be denoted as $\mathbf{X} \in \mathbb{R}^{T \times C}$, with T timesteps and C channels. We apply a sliding window with patch length L and stride S independently to each channel. This yields a grid of patches $\mathbf{P} \in \mathbb{R}^{C \times N_p \times L}$, where $N_p = \lfloor (T - L)/S \rfloor + 1$ is the number of temporal patches per channel.

We employ a window of $T = 1000$ timesteps, $L = S = 20$, and $C = 16$, yielding to 50 tokens per channel (N_p) and a total sequence length of 800 tokens (N).

To form the input sequence for the Transformer, we flatten the channel and temporal dimensions, resulting in a total sequence length of $N = C \times N_p$. Each patch $\mathbf{P}_{c,i}$ (where c is the channel index and i is the patch index) is mapped to a

latent embedding of dimension d_e via a *shared* learnable linear projection $\mathbf{W}_{\text{proj}} \in \mathbb{R}^{d_e \times L}$. The resulting token sequence $\mathbf{E} \in \mathbb{R}^{N \times d_e}$ consists of embeddings:

$$\mathbf{E}_k = \mathbf{W}_{\text{proj}} \mathbf{P}_{c,i}^\top, \quad (1)$$

where the token index k corresponds to the flattened arrangement of channel-time pairs (c, i) . We do not add learnable positional embeddings; instead, we inject positional information via Rotary Position Embeddings (RoPE) [33] within the attention blocks.

2) Architecture:

We adopt an Encoder-Decoder architecture. The Encoder (see Fig. 1) consists of 8 identical layers, based on pre-LayerNorm Transformer encoder [34], [35], with 3 attention heads and an embedding dimension of 192, analogous to the configuration used in EfficientViT [36].

We adopt a RoPE approach, which introduces position information by rotating query and key vectors in 2D planes instead of adding a position vector; such a method has already been adopted for biosignals [13], [14], [37].

During pre-training, the Encoder's output is passed to a lightweight Decoder (3.9k parameters), consisting of a linear layer that outputs a sequence $\hat{\mathbf{P}}$, which is a reconstruction of the original patch sequence \mathbf{P} . Our approach draws inspiration from SimMIM [38], which demonstrates that a *minimal* reconstruction head (e.g., a single linear layer) is sufficient for

effective self-supervised pre-training.

The use of a lightweight decoder is intentional: placing the full reconstruction burden on the encoder forces it to learn semantically rich and task-agnostic representations, rather than relying on a high-capacity decoder to compensate for missing information. This design strategy is supported by recent survey analyses in the masked image modeling (MIM) literature: shallow decoders tend to limit shortcut learning and encourage the formation of stronger latent representations within the encoder [39]. As a result, the learned features exhibit improved generalization across downstream tasks and recording conditions. Further details on the model's parameters are reported in Table I (left).

3) Pre-training objectives: We adopt a random-masking approach [38], where a random subset \mathcal{M} of tokens is replaced by a learnable $[\text{MASK}]$ token. Applying the masking over each patch enforces contextual inference over tens of milliseconds (physiologically meaningful burst segments), rather than trivial gap filling. We adopt a masking ratio of 50% as in previous works [30], [32].

We employ the Smooth L1 Loss function as reconstruction objective between masked and original patches, as in [13]. We define the following loss components:

$$\mathcal{L}_{\text{masked}} = \frac{1}{|\mathcal{MASK}|} \sum_{(c,i) \in \mathcal{MASK}} \text{SmoothL1}(\mathbf{P}_{c,i}, \hat{\mathbf{P}}_{c,i}), \quad (2)$$

$$\mathcal{L}_{\text{visible}} = \frac{1}{|\mathcal{M}|} \sum_{(c,i) \in \mathcal{M}} \text{SmoothL1}(\mathbf{P}_{c,i}, \hat{\mathbf{P}}_{c,i}), \quad (3)$$

where \mathcal{MASK} and \mathcal{M} are the sets of masked and visible patches, respectively. To avoid overfitting on unmasked input, the loss on visible patches is reduced by a factor of 0.1. The final reconstruction objective is given by:

$$\mathcal{L}_{\text{total}} = \mathcal{L}_{\text{masked}} + 0.1 \cdot \mathcal{L}_{\text{visible}} \quad (4)$$

Additional details on pre-training set-up are provided in Table I (right).

TABLE I
HYPERPARAMETERS FOR MASKED EMG PRE-TRAINING.

Hyperparameter	Value	Setup	Value
Transformer Encoder			
Timesteps	1000	Batch size	512
Patch size ($H \times W$)	1×20	Peak LR	1×10^{-4}
Channels	16	Minimum LR	1×10^{-6}
Embed dim	192	Optimizer (β_1, β_2)	AdamW (0.9, 0.98)
Layers	8	LR schedule	Cosine
Heads	3	Weight decay	0.01
QKV bias	Yes	Epochs / warm-up	50 / 10
QK norm	No	Grad accum batches	8
MLP ratio	4.0	Grad clip	3
MLP size	768	Mask ratio	0.5
Attn drop	0.1	Max seq length	1000
Proj drop	0.1	LR: learning rate	
Drop-path	0.1		
Decoder			
Decoder embed dim	192		

All experiments are implemented in Python 3.10 using PyTorch Lightning and Hydra for modularity, configurability,

and reproducibility. The proposed foundation model is trained on the CSCS Alps HPC infrastructure using NVIDIA GH200 GPUs, employing a single node with 4x NVIDIA GH200 GPUs in Distributed Data Parallel (DDP) mode.

4) Pre-training Datasets: For model pre-training, we employ three publicly available datasets, with a summary provided in Table II.

TABLE II
PRE-TRAINING EMG DATASETS.

Dataset	#Sub	f_s [Hz]	#Ch	Size [GB]	Placement
Ninapro DB6 [22]	10	2000	14	20.3	Forearm
Ninapro DB7 [22]	22	2000	12	30.9	Forearm
EMG2Pose [12]	192	2000	16	431	Wrist

Ninapro DB6 [22] contains sEMG from 10 subjects performing 7 hand grasp types, each repeated 12 times over 5 separate recording days. Signals were acquired with Trigno sensors (14 channels, 2 kHz sampling rate), placed on the forearm. The total dataset size is 20.3 GB.

Ninapro DB7 [40] contains data from 20 intact subjects and 2 transradial amputees, performing 40 movements spanning isolated finger/wrist actions and grasp patterns. Data were collected using Trigno sensors (12 channels, 2 kHz sampling rate), placed on the forearm. The total dataset size is 30.9 GB.

EMG2Pose [12] contains data from 193 participants, performing 29 different hand motions. Data were recorded with a custom wristband (16 channels, 2 kHz sampling rate). The total dataset size is 431 GB.

5) Pre-training Data Processing: EMG data are pre-processed using a Butterworth band-pass filter (4th order, 20 – 450 Hz), followed by a notch filter (50 Hz), as in [13]. Min-Max, channel-wise normalization ($[-1, 1]$ range) is applied. Each recording is then segmented into fixed-length windows of 1000 samples (500 ms at 2 kHz) with 50% overlap, providing sufficient temporal context [41] [42] while controlling computational load.

Datasets with fewer than 16 channels are zero-padded. Given that each training batch might contain data from each dataset, this approach ensures consistency in the number of channels per batch.

We did not apply any data augmentation in line with previous works [13], [14] which already showed SoA performances. Additionally, given the small model size (3.6 M parameters) and the limited effect of data augmentation shown in scaling-laws regimes [43], we rely on the sample-efficiency of the architecture rather than increasing artificially the data variance.

B. Downstream Tasks

1) Pipeline Overview: For all downstream tasks, the Encoder architecture described in Sec. III-A.2 is retained without modification, while the Decoder used during pretraining is removed.

The Encoder output is processed through a channel-fusion and temporal pooling module (detailed in the following subsection), after which the resulting representation is fed into

task-specific prediction heads, whose specifics are provided in the corresponding downstream task sections (see Sec.III-B.2).

For each temporal patch index p , the Encoder outputs a set of channel-wise embeddings $\{\mathbf{z}_{c,p} \in \mathbb{R}^{d_e}\}_{c=1}^C$. We fuse these representations by concatenation, producing a per-patch vector $[\mathbf{z}_{1,p} \| \cdots \| \mathbf{z}_{C,p}] \in \mathbb{R}^{C \times d_e}$. This choice preserves electrode-specific information by retaining the per-channel structure, allowing the downstream linear head to assign independent weights to each channel. Ablation studies confirmed that concatenation consistently outperforms mean-based fusion.

Following channel fusion, we apply temporal average pooling: $\mathbf{h}_c = \frac{1}{N_c \cdot p} \sum_{p=1}^{N_p} \mathbf{z}_p$, $\mathbf{z}_p \in \mathbb{R}^{C \times d_e}$. This aggregation step yields a compact representation while preserving discriminative spatiotemporal structure, and it serves as the input to the final linear task-specific head.

2) Downstream Tasks: The pretrained encoder is evaluated on the datasets listed in Table III. We classify the downstream tasks into three categories: Hand Gesture Classification, Hand Kinematic Regression, and Speech Synthesis and Recognition.

Downstream 1: Hand Gesture Classification

This task consists of classifying different types of hand-wrist movements and is evaluated on the following datasets:

- *Ninapro DB5* [16] contains data collected from 10 intact subjects, using two Thalmic Myo Armbands (16 channels, 200 Hz). The task consists of classifying 52 hand-wrist movements.
- *EPN-612* [17] contains data collected from 612 subjects, using the Myo Armband (8 channels, 200 Hz). The task consists of classifying 5 hand movements.
- *UC Irvine* [18] contains data from 36 subjects (8 channels, 200 Hz). The task consists of classifying 7 movements.

Datasets are pre-processed using a band-pass filter (Butterworth, 4th order, [20 – 90] Hz), followed by a notch filter (50 Hz). Then, windowing is applied. We perform an ablation over two different window sizes: 200 ms with 25% overlap, and 1000 ms with 25% overlap. After filtering and windowing, each dataset is normalized using per-channel z -score normalization.

Compared to the pre-training, datasets with fewer than 16 channels are not zero-padded because tokenization is performed on a per-channel basis; thus, having fewer channels simply results in fewer tokens, eliminating the need for padding.

For Ninapro DB5, we perform a per-repetition split as in [13], each recording contains six repetitions, and for each subject, we assign whole repetitions to a single split so that no subject data overlaps across splits. Specifically, repetitions 1, 3, 4, and 6 are used for training, repetition 2 for validation, and repetition 5 for testing.

The UCI EMG dataset is split by subject index into three disjoint groups: subjects 1–24 are used for training, subjects 25–30 for validation, and subjects 31–36 for testing. Only subjects 11 and 30 performed the "extended palm" gesture, so they were excluded from all data splits, hence reducing the total number of gestures to 6.

For EPN-612, we preserve the original per-user organization [17] and derive splits per user. When constructing the testing

split, held-out examples per user are used, ensuring that samples from the same user do not appear across train, validation, or test splits.

The model head architecture is lightweight and consists of a single fully connected linear layer that maps the pooled feature representation (max $192 \times N_c$, N_c = number of channels) to the final class logits (N_o , N_o = number of outputs). No additional hidden layers, normalization modules, or nonlinearities are used in the head. Hence, the model head has a maximum of $192 \times N_c \times N_o$ parameters. For training, we employ the cross-entropy loss computed over the predicted logits and the corresponding ground-truth labels. We evaluate performance using Accuracy, F1-score, and AUROC, with the respective definitions given below:

$$\begin{aligned} \text{Accuracy (micro)} &= \frac{1}{N} \sum_{i=1}^N \mathbb{1}(\hat{y}_i = y_i), \\ \text{Accuracy (macro)} &= \frac{1}{K} \sum_{k=1}^K \frac{\text{TP}_k + \text{TN}_k}{\text{TP}_k + \text{TN}_k + \text{FP}_k + \text{FN}_k}, \\ \text{F1-score (macro)} &= \frac{1}{K} \sum_{k=1}^K \frac{2 \text{TP}_k}{2 \text{TP}_k + \text{FP}_k + \text{FN}_k}, \\ \text{AUROC (macro)} &= \frac{1}{K} \sum_{k=1}^K \text{AUROC}_k. \end{aligned}$$

where \hat{y}_i is the predicted class, y_i the ground-truth label, and TP_k , FP_k , FN_k denote true positives, false positives, and false negatives for class k .

We repeat each experiment five times using five distinct random seeds and report the mean performance across runs.

An additional dataset is also considered as part of this downstream task:

- *Generic Neuromotor Interface* [6] contains data collected from 4900 participants, recorded with a custom wristband developed by Meta Reality Labs (16 channels, 2kHz). Data from only 100 subjects are publicly available [44], randomly selected from the entire cohort.

Specifically, we tackle the *discrete-gesture* task presented in the original work, consisting of the classification of 9 fine finger movements. We treat this task separately, compared to the three other datasets presented above, owing to substantial methodological differences in data processing and evaluation protocols.

No pre-processing is applied to the data. Signals are windowed using 8000 ms windows, no overlap. The train dataset contains 80% of data from each subject for train, 10% for validation, 10% for test. The model head consists of a single linear layer, with input size of $N_c \times 192$, output size 9. We employ the Cross-Entropy Loss function, and we conduct 5 runs with 5 seeds values.

We evaluate the performance with the Classification Error Rate (CLER), defined as *the proportion of ground-truth labels for which the matching prediction is incorrect* [6]. The CLER is computed per-gesture and reported as the average across

TABLE III
SUMMARY OF DOWNSTREAM EMG DATASETS.

Dataset	#Subj.	f_s [Hz]	Ch	Size [GB]	Placement	Window size (ms)	Pre-Processing	Metrics
Ninapro DB5 [16]	10	200	16	0.2	Forearm	200, 25% overlap 1000, 25% overlap	BP 20–90 Hz → NC 50 Hz	Accuracy, F1, AUROC
EPN-612 [17]	612	200	8	5.5	Forearm	200, 25% overlap 1000, 25% overlap	BP 20–90 Hz → NC 50 Hz	Accuracy, F1, AUROC
UC Irvine [18]	36	200	8	0.32	Forearm	200, 25% overlap 1000, 25% overlap	BP 20–90 Hz → NC 50 Hz	Accuracy, F1
Generic Neuromotor Interface [6]	100	2000	16	31.1	Hand/Arm	8000 (no overlap)	HP (40Hz)	CLER
Ninapro DB8 [19]	12	2000	16	23.6	Forearm	200	—	MAE
Gaddy Silent Speech [20]	1	1000	8	3.9	Face/Neck	≈3000	Series of NC ([60, ..., 420]Hz → HP 2Hz → downsampling)	WER

BP: band-pass filter; NC: notch filter.

gestures. The CLER formula is given by:

$$\text{CLER} = \frac{1}{|N_G|} \sum_{g \in G} \left(1 - \frac{C_{g,g}}{\sum_{p \in G} C_{g,p}} \right).$$

where N_G is the total number of gestures, $g \in N_G$, $C_{g,g}$ is the number of correct predictions for gesture g and $\sum_{p \in G} C_{g,p}$ is the total number of ground-truth occurrences of g . In the original work, the architecture is tested on the full sequence of EMG data. The architecture proposed in this work cannot process the entire sequence due to quadratic complexity. We adopt a windowed inference approach, which involves sliding a window of 8s, with 2s stride. In order to compare the original LSTM architecture with the proposed Transformer model, the same windowed inference strategy is applied to the LSTM during evaluation, and both results are reported.

Downstream 2: Hand Kinematic Regression

This task consists of predicting continuous hand and wrist movement (regression task). We employ the *Ninapro DB8* [19] dataset. It contains EMG data collected from 12 subjects (16 channels, 2 kHz), with 3 sessions per subject. Data were collected with an instrumented glove from ground-truth. The task consists of regressing 5 Degrees of Freedom (DoFs), defined as linear combinations of the 18 DoFs of the instrumented glove [45].

Each EMG channel is independently standardized using z -score normalization. No filtering is applied since the original data is already released filtered (4th order bandpass Butterworth filter, [10–500 Hz]). The glove data undergo a mapping from 18 Degrees of Freedom (DoF) to 5 Degrees of Actuation (DoA). Both EMG and glove data are then segmented into fixed-size windows with no overlap in two different settings: 1000ms and 200ms.

Following the author's recommendations, we consider the first two sessions for training, the third as validation. The model head architecture (788 K parameters) consists of a compact series of pointwise and depthwise convolutions, followed by upsampling to a fixed length. We employ the L1 loss function.

We report the mean absolute error (MAE), root mean squared error (RMSE), and the coefficient of determination R^2 , defined as:

$$\text{MAE} = \frac{1}{N} \sum_{i=1}^N |y_i - \hat{y}_i|.$$

$$\text{RMSE} = \sqrt{\frac{1}{N} \sum_{i=1}^N (y_i - \hat{y}_i)^2}.$$

$$R^2 = 1 - \frac{\sum_{i=1}^N (y_i - \hat{y}_i)^2}{\sum_{i=1}^N (y_i - \bar{y})^2}.$$

where y_i are the true values, \hat{y}_i the predicted values, and $\bar{y} = \frac{1}{N} \sum_{i=1}^N y_i$. We conduct 5 runs, with 5 random seed values, and report the average.

Downstream 3: Speech Synthesis and Recognition

We employ the open-vocabulary dataset presented by Gaddy et al. [20]. It comprises 8 channels, sampled at 1000 Hz, recorded using wet electrodes, placed on the face. Data were collected from one subject in multiple sessions while reading pieces of public domain books. The dataset contains both *vocalized* (i.e., normal articulation with sound production) and *silent* (i.e., articulation without sound production) EMG data. In the vocalized setting, EMG data were recoded together with a microphone, serving as ground truth. For the silent setting, audio recorded during vocalized experiments is aligned to the corresponding silent EMG data using the dynamic time warping algorithm [20]. The publicly available dataset contains already-aligned data.

For both tasks, we adopt the same data processing pipeline as in [46]. A cascade of notch filters is applied to suppress the first six harmonics of power line frequency ([60, 240, ..., 420] Hz). Additionally, a high-pass filter (Butterworth, 2 Hz, 3rd order) is applied. Data are downsampled (from 1000 Hz to 516.79 Hz, matching the processing pipeline in [47]).

For this dataset, we tackle two sub-tasks: *Speech Synthesis* and *Speech Recognition*. *Speech Synthesis* aims at producing audio from EMG data. The full speech production pipeline consists of three steps: a Transduction Model, a Vocoder, and an Automatic Speech Recognition (ASR) model. First, a Transduction model is trained to reconstruct audio target features (Mel-Frequency Cepstral Coefficients, MFCC). It consists of 3 residual blocks (as in [46]) that downsample

the input (1600 samples to 200 samples). The 200 samples are the input to the pre-trained Transformer Encoder; we add relative positional embeddings, following [46]. A lightweight linear head follows, with an input dimension of $192 \times N_c$, output dimension of 26 MFCC.

The model is trained using as loss function the mean of pair-wise MFCC distances (L) plus an auxiliary phoneme loss (L_{phon}) [46]. In the case of silent EMG data, DTW is used to align the MFCC features predicted from silent EMG to the sequence of target MFCC features obtained from a parallel vocalized recording. Predicted MFCC audio features are fed to a HiFi-GAN [48] vocoder, which converts the audio features into raw audio waveforms. We adopt the publicly available [47] pre-trained HiFi-GAN vocoder from Gaddy's work [20], without any fine-tuning.

For model evaluation, we employ the Wav2Vec2 [49] ASR model, pretrained on LibriSpeech (English Language) within SpeechBrain [50].

Speech Recognition consists of recognizing speech (words) without any acoustic output, yielding text as output. Producing text directly from EMG signals is preferable to first synthesizing audio and then applying an ASR system: direct text prediction serves as a more efficient surrogate for human intelligibility, avoids the intermediate audio-generation stage, and yields improved recognition accuracy [51]. Moreover, EMG-to-text models do not require an additional vocoder for speech production, substantially reducing model size and computational load. This makes the approach more suitable for deployment on resource-constrained embedded platforms.

The model architecture is the same as before (Residuals, pre-trained Transformer Encoder and linear layer with softmax). The input to the final linear layers has a dimension of $N_c \times 192$, the output dimension is 37 (26 lowercase English letters, 10 digits, and space character). We adopt the Connectionist Temporal Classification (CTC) [52] loss function with a 4-gram language model trained on the LibriSpeech dataset [53]. During inference, beam search is applied to explore the search space and select the paths with the highest likelihood.

The dataset is split as in Gaddy *et al.* [46]. Training is performed using both silent and vocalized EMG recordings; testing is performed on silent data. Data are split into training, validation, and test sets using the original index file containing pairs of book and sentence indexes. Each utterance is assigned to one of the three splits. During training, a size-aware sampler is used to group examples, together producing compact batches and a more efficient training stage.

For both tasks, we use the Word Error Rate (WER) as the evaluation metric, defined as

$$WER = \frac{S + D + I}{N},$$

where S , D , and I denote the number of substitution, deletion, and insertion errors, respectively, and N is the total number of words in the reference transcription.

3) Experimental Settings: All downstream experiments are performed with the same hyperparameters, as per Table IV.

We evaluate the downstream tasks under two different settings: (i) *Full-supervised (FS)*, where the model is trained

TABLE IV
HYPERPARAMETERS FOR MODEL FINE-TUNING.

Hyperparameter	Value
Batch size	32
Peak LR	5×10^{-4}
Minimum LR	1×10^{-5}
LR scheduler	Cosine
Optimizer (β_1, β_2)	AdamW (0.9, 0.98)
Weight decay	0.01
Max training epochs *	50
Warm-up epochs	5
Drop-path	0.10
Layer-wise LR decay	0.90
Label smoothing	0.10

LR: learning rate;

* Early stopping is adopted, with patience of 7 epochs (validation set).

from scratch on the task-specific dataset without relying on pre-trained weights; (ii) *Full Finetuning (FT)*, where the entire model is fine-tuned using layer-wise learning rate decay to avoid catastrophic forgetting [54].

C. Model Deployment

We deploy the TinyMyo on the GreenWaves Technologies GAP9 [55] processor, a multi-core RISC-V MCU designed for ultra-low-power edge AI. The architecture features a hierarchical memory organization consisting of a large off-chip L3 (HyperRAM), a 1.5 MB on-chip L2 (shared memory), and a 128 kB L1 (Tightly Coupled Data Memory) shared among a cluster of 8 compute cores and a dedicated cluster controller.

To enable the execution of the Transformer-based architecture, which exceeds the on-chip L2 capacity in terms of parameters and intermediate activation maps, we developed a custom deployment toolchain that implements a hierarchical streaming architecture.

Unlike traditional MCU inference engines that require the full model to reside in on-chip memory, our approach treats L2 as a streaming buffer. We implement a multi-level tiling strategy:

- **L3 → L2:** Large tensors (weights and activations) are stored in external L3 memory. They are retrieved into L2 slabs on demand. For example, in linear and multi-head self-attention layers, weights are streamed slab by slab to prevent memory overflows.
- **L2 → L1:** Computation is performed by moving data from the L2 slabs into L1 tiles. The cluster controller orchestrates high-bandwidth DMA transfers, while the 8 worker cores execute compute kernels in parallel.

To minimize the overhead of external memory access, we implement a double-buffered pipeline. While the worker cores compute the current slab (N), the cluster controller asynchronously pre-fetches the next slab (N+1) from L3 to L2 or from L2 to L1. This effectively hides the latency of data movement behind the compute-bound operations of the transformer blocks.

We apply INT8 quantization to convert all weights and activations from FP32 to 8-bit fixed-point representations. All intermediate tensors, including those in MHSA (with integer softmax) and GELU/LayerNorm, are stored and processed

TABLE V
FLOPs BREAKDOWN

Experiment	FLOPs
Model Pretraining (Encoder + Decoder)	4.001 G
Ninapro DB5	4.813 G
EPN-612	1.916 G
UCI-EMG	1.916 G
Generic Neuromotor	13.6315 G
Ninapro DB8	4.852 G
Speech Production	1.0956 G
Speech Recognition	1.0921 G

in INT8 format, with only the LayerNorm scale and shift parameters (γ and β) retained in FP32. The only remaining FP32 operation is the final classification layer, which consumes INT8 inputs and weights but accumulates to FP32 logits to enable a direct comparison with the original FP32 baseline; in principle, this layer could also be executed entirely in INT8.

To maximize the utilization of the limited 1.5 MB L2 memory, we employ an offline liveness analysis pass. Instead of dynamic allocation, the deployment flow calculates a static memory arena. Tensors are assigned offsets within this arena based on their execution lifetime, allowing mutually exclusive buffers (e.g., non-overlapping intermediate feature maps) to share the same physical memory addresses.

To maintain numerical fidelity while avoiding costly floating-point operations, all transformer primitives are implemented in fixed-point arithmetic [56]. We use integer-only variants of softmax (i-Softmax), layer normalization (i-LayerNorm), and GELU activation (i-GELU), which leverage lookup tables and multiplicative inverses to approximate their floating-point counterparts with minimal error.

As proof of concept, we deploy the *Hand Gesture Classification* downstream task on the *NinaPro DB5* dataset.

IV. RESULTS

A. Pre-training

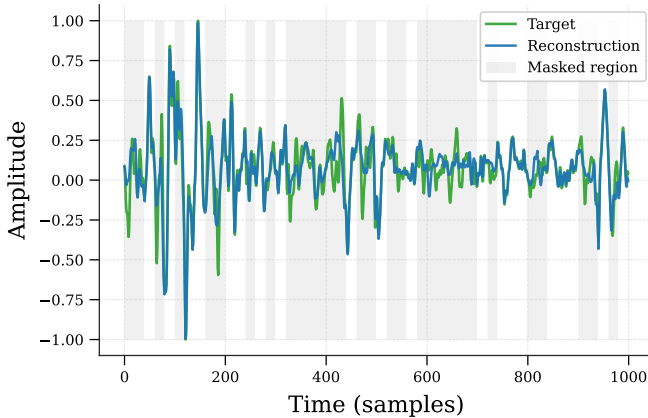


Fig. 2. Example of reconstruction for a EMG window by the proposed Foundation model. Grey areas correspond to the masked signal regions, white areas to the unmasked.

Figure 2 shows an example of the reconstruction of the EMG signal performed by the model.

With a parameter count of only 3.6 million (with only 0.1% of parameters for the decoder), in line with previous works [14], our model demonstrates that high reconstruction fidelity can be maintained even under a strict parameter budget and low computational requirements. A breakdown of the floating-point operations (FLOPs) is available in Table V.

B. Down-stream Tasks Results

1. Hand Gesture Classification: Table VI reports the results obtained on the *Ninapro DB5* [16], *EPN-612* [17] and the *UC Irvine* [18] datasets, offering a comparison with previous works based on foundation models.

On the *NinaPro DB5* dataset, the fine-tuned model trained with a window size of 200 ms achieves state-of-the-art performance, with an accuracy of $89.41 \pm 0.16\%$ and an F1-score of $77.97 \pm 0.59\%$. Fine-tuning the pre-trained model yields an improvement of approximately 7.5% in accuracy compared to training from scratch. Moreover, using a window size of 200 ms substantially improves performance over 1000 ms (around 10% for the fine-tuned model). This effect is consistent with the acquisition protocol, which comprises 52 different movements. Since, during data pre-processing, we did not remove the transition periods between gestures in order to emulate real-life use cases, using shorter windows reduces the likelihood that segments overlapping these transitions are assigned incorrect gesture labels, thereby mitigating label noise. It must be noted that this dataset exhibits a substantial imbalance toward the *rest* class. To ensure a fair comparison with prior work, we did not apply any rebalancing techniques during training or evaluation. We assume that earlier studies reported the micro accuracy, as no alternative definition was explicitly stated. When computing the macro-averaged accuracy score, the accuracy decreases to $75.80 \pm 0.62\%$, which reflects the imbalance in the dataset.

On the *EPN-612* dataset we achieve SoA results (window size of 1000ms, with a global accuracy (FT) of $96.74 \pm 0.09\%$, F1-score of $96.74 \pm 0.08\%$ and AUROC of $99.70 \pm 0.02\%$.

On the *UCI-EMG* dataset, the best performance is obtained with an input window of 1000 ms, achieving an accuracy of $97.56 \pm 0.32\%$, an F1-score of $97.55 \pm 0.31\%$, and an AUROC of $99.93 \pm 0.02\%$. The performance of the model trained from scratch is comparable to that obtained with the pre-trained TinyMyo encoder, which we attribute to the relative simplicity of this downstream task.

For the *Generic Neuromotor Interface - discrete gesture task* [6], we achieve a CLER of 0.144 ± 0.004 on the model trained from scratch, which compares to the 0.1596 (obtained with our windowed inference method, see Sec. III-B.2) obtained with the LSTM model proposed in the original work, however with $\approx 44\%$ reduction in model size. In this case, the results achieved with the pre-trained Foundation Model are worse (0.153 ± 0.006), which we attribute to the intrinsic nature of the problem: to emulate the sequential processing behaviour of the original stacked LSTMs, we imposed a causal mask on the attention mechanism. This constraint restricts our architecture,

TABLE VI
HAND GESTURE CLASSIFICATION TASK — COMPARISON WITH STATE OF THE ART.

Model	Params	NinaPro DB5			EPN-612			UCI-EMG		
		Acc	F1	AUROC	Acc	F1	AUROC	Acc	F1	AUROC
Moment (as in [13])	385M	86.41	74.42	N.A.	90.87	90.16	N.A.	90.45	91.75	N.A.
Moment (as in [14])		86.41 \pm 1.13	76.84 \pm 1.95	99.34 \pm 0.12	93.83 \pm 0.76	93.75 \pm 0.82	99.63 \pm 0.09	92.79 \pm 0.64	91.24 \pm 0.71	99.47 \pm 0.11
OTIS (as in [13])	45M	85.31	72.61	N.A.	87.55	88.03	N.A.	90.62	89.28	N.A.
OTIS (as in [14])		81.79 \pm 1.56	60.81 \pm 2.43	98.24 \pm 0.22	84.82 \pm 1.24	85.01 \pm 1.18	97.22 \pm 0.31	89.14 \pm 0.98	89.49 \pm 1.03	98.73 \pm 0.18
PhysioWave-Small [13]	5M	84.78	72.54	N.A.	93.12	93.40	N.A.	90.35	89.51	N.A.
WaveFormer [14]	3.10M	87.53 \pm 0.92	74.66 \pm 1.78	99.35 \pm 0.10	95.21 \pm 0.68	95.22 \pm 0.71	99.70 \pm 0.07	93.10 \pm 0.58	93.20 \pm 0.62	99.60 \pm 0.08
TinyMyo (FS), 200ms	3.6M	81.94 \pm 1.22	58.52 \pm 3.17	96.49 \pm 0.20	74.33 \pm 0.72	74.31 \pm 0.72	93.80 \pm 0.24	93.63 \pm 0.64	93.58 \pm 0.63	99.52 \pm 0.11
TinyMyo (FT), 200ms	3.6M	89.41 \pm 0.16	77.97 \pm 0.59	98.59 \pm 0.13	78.54 \pm 0.32	78.50 \pm 0.35	95.20 \pm 0.18	94.08 \pm 0.72	94.07 \pm 0.70	99.50 \pm 0.19
TinyMyo (FS), 1000ms	3.6M	72.42 \pm 0.31	32.45 \pm 1.02	94.89 \pm 0.30	95.18 \pm 0.10	95.17 \pm 0.10	99.51 \pm 0.03	97.56 \pm 0.32	97.55 \pm 0.31	99.93 \pm 0.02
TinyMyo (FT), 1000ms	3.6M	79.22 \pm 0.93	50.89 \pm 2.50	95.80 \pm 0.62	96.74 \pm 0.09	96.74 \pm 0.08	99.70 \pm 0.02	97.23 \pm 0.70	97.22 \pm 0.70	99.93 \pm 0.02

Notes: PhysioWave [13] use windows of ≈ 1953 ms. EMG data are upsampled at 2kHz and a fixed window size of 1024 samples is used. WaveFormer [14] uses a fixed window of 1024 samples; no information is available on whether resampling is applied.
FS: model trained from scratch, FT: fine-tuning pretrained model.

TABLE VII
DISCRETE GESTURE CLASSIFICATION TASK- COMPARISON WITH SOA

Model	Params	CLER	Inference Method
LSTM, Kaifosh [6] ^(a)	6.4M	0.1819	Full sequence
LSTM, Kaifosh [6] ^(b)	6.4M	0.1596	Windowed
TinyMyo - FS	3.6M	0.144 \pm 0.004	Windowed
TinyMyo - FT	3.6M	0.153 \pm 0.006	Windowed

^(a): Full sequence results obtained with methods provided by the authors ([6])
^(b): results obtained with the same model as in ^a, with the windowed-inference method described in the corresponding Methods section. FS: model trained from scratch, FT: fine-tuning pretrained model

initially optimized for bidirectional dependency modelling, to a strictly left-to-right context, leading to a degradation in the effectiveness of the pre-trained weights when the future information on which they were originally trained is no longer available. Table VII reports a summary of the results.

We note that our work is the first to include this dataset among the downstream tasks and to propose an alternative architecture compared to the one employed in the original work.

2. Hand Kinematic Regression: Table VIII reports the result for the Hand Kinematic Regression task.

TABLE VIII
GESTURE REGRESSION TASK ON NINAPRO DB8 - COMPARISON WITH SOA

Model	Params	MAE $^{\circ}$	RMSE $^{\circ}$	R 2
TEMPONet TCN, Zangheri [57]*	<500K	6.89	—	—
Event-based Lin. Reg., Zangheri [58]*	—	8.8 \pm 2.3	—	—
DNKF, Bao [59]**	—	—	13.5	—
TinyMyo - FS, 200 ms (***)	3.8M	9.36 \pm 0.05	15.28 \pm 0.09	0.52 \pm 0.00
TinyMyo - FT, 200 ms	3.8M	9.40 \pm 0.14	14.83 \pm 0.14	0.55 \pm 0.01
TinyMyo - FS, 1000 ms	3.8M	9.01 \pm 0.07	13.95 \pm 0.16	0.59 \pm 0.01
TinyMyo - FT, 1000 ms	3.8M	8.77 \pm 0.12	13.35 \pm 0.15	0.62 \pm 0.01

* 5 DoFs, subject-specific model; ** 3 DoFs, subject-specific model;

*** 5 DoFs, across-subject model;

FS: model trained from scratch, FT: fine-tuning pretrained model

We obtain a MAE of $8.77 \pm 0.12^{\circ}$, with a window size of 1000ms. This value is higher than the result reported

by Zangheri et al. [57] ($MAE = 6.89^{\circ}$), primarily due to differences in both the training and evaluation protocols. In our setting, the model is trained in an *across-subject* regime using data aggregated from all participants, while prior work trained *subject-specific* models, i.e., one model per individual. Learning a single model that generalizes across subjects is substantially more challenging because of inter-subject variability in muscle physiology, electrode placement, and EMG signal morphology.

3. Speech Recognition: Table IX reports the results for the Speech Synthesis Task.

Our model achieves a WER (FT) of $33.54 \pm 1.12\%$, in line with previous works (SoA WER is 32%, achieved by Ren et al. [60]). Compared to previous solutions, our Transduction model offers a significant reduction in parameter size, with 62.5% reduction compared to Scheck et al. [61] and 91.7% reduction compared to Gaddy et al. [46].

The reported number of parameters accounts only for Transduction model (encoder and model head). The number of parameters for the pre-trained Hi-Fi Gan vocoder is 13.92M (same as in [46], [60]).

TABLE X
SILENT SPEECH RECOGNITION TASK - COMPARISON WITH SOA

Method	Params	WER
Transformer, Gaddy [51]	54 M	28.8%
MONA, Benster [66] ^(a)	n.a.	22.2%
MONA LISA, [66] ^(a)	n.a.	12.2%
TinyMyo - FT	4.5 M	33.95% \pm 0.97%

^(a): Multimodal model

FT: fine-tuning pretrained model

Table X reports the results for the Speech Recognition Task. Given the superior performance of the fine-tuned model compared to training from scratch in the Speech Production task, and the identical architecture adopted for the vocoder, in this case, we run the experiments only for the full fine-tuning setting. We achieve a WER of $33.95\% \pm 0.97\%$, higher

TABLE IX
SILENT SPEECH SYNTHESIS TASK – COMPARISON WITH SOA

Method	Transduction Model		Vocoder		ASR	WER
	Model	Params [M]	Model	Params [M]		
Transformer, Gaddy [46]	CNN + Transformer	54	HiFi-GAN	13.92	DeepSpeech	36%
Diff-ETS, Ren [60]	as [46] + Diffusion Probabilistic Model	>54 ^(a)	HiFi-GAN	13.92	Whisper Medium (EN)	32%
SU-E2S, Scheck. [61]	HuBERT-Soft	N.A.	HiFi-GAN	13.92	Whisper Medium (EN)	40%
DiffMV-ETS [62]	DiffMV-ETS	≈ 66 ^(b)	BigVGAN	112	Distil-Whisper-v3	N.A.
EMGVox-GAN [63]	as [46]	as [46]	EMGVox-GAN	12	N.A.	36%
SWS, Lee [64]	as [46]	54	Sovits-SVC	N.A.	Whisper Medium (EN)	38%
TinyMyo – FS	Transformer Encoder	4.5M	HiFi-GAN	13.92	Wav2Vec2 [65]	35.23±0.22%
TinyMyo – FT	Transformer Encoder	4.5M	HiFi-GAN	13.92	Wav2Vec2 [65]	33.54±1.12%

^(a) = estimated. The authors employ the same Transduction model as in Gaddy [46], followed by a Diffusion Model (including residual blocks, attention and convolutional layers)

^(b) = estimated as sum of speaker encoder (6M), prior encoder (30M), and diffusion decoder (30M)

FS: model trained from scratch, FT: fine-tuning pretrained model

compared to 28.8% reported of Gaddy et al. [51], however, with a 91.7% reduction in parameter count.

The MONA LISA model [66] achieves a WER of 12.2%. However, this performance relies on a multimodal training setup, where both EMG and audio data are jointly used. Moreover, MONA LISA is a large-scale language model, which poses practical limitations for real-time deployment and edge applications due to its substantial computational footprint and memory requirements.

C. Model Deployment

We deploy TinyMyo on the GAP9 microcontroller, as described in Section III-C. The model comprises 3.56 million parameters, with the majority residing in the 8 transformer blocks. Each block contains a multi-head self-attention (MHSA) layer with 3 heads and a feed-forward network (FFN) with an expansion ratio of 4.

Table XI reports a computational cost breakdown of the deployed model for one Transformer Block. We can observe that the computational cost is dominated by the MHSA QK/AV operations (40% of total MACs) and the MLP projections (40% of total MACs). In particular, the QK and AV terms scale as $\mathcal{O}(N^2d)$ with the sequence length $N = 800$, making them the asymptotic computational bottleneck of the Transformer block.

With GAP9 operating at 370 MHz, utilizing all 9 cores in the cluster to execute TinyMyo computations in parallel, we achieve an inference in around 12.2 seconds at only 0.44J with an average power-envelope of 36.45mW.

TABLE XI
COMPUTATIONAL COST PER TRANSFORMER BLOCK

Component	MACs	% of Total
MHSA Q/K/V projections	88M	15%
MHSA QK scores	123M	20%
MHSA AV context	123M	20%
MHSA output projection	29M	5%
MLP FC1	118M	20%
MLP FC2	118M	20%

Notes: QK scores and AV context is $(800 \times 800 \times 3 \text{ heads})$. FC1 and FC2 are $192 \rightarrow 768$ and $768 \rightarrow 192$ with $4 \times$ MLP expansion factor.

V. CONCLUSION

In this work, we presented TinyMyo, the first compact EMG FM capable of broad generalization across diverse downstream tasks and real-time edge deployment on an ultra-low-power microcontroller.

TinyMyo is based on a Transformer-encoder architecture, with a size of 3.6 million parameters. The model is pre-trained using heterogeneous EMG data, collected from platforms with different numbers of channels and from diverse body locations.

TinyMyo achieves SoA performance across multiple downstream tasks. For gesture recognition, we obtain SoA accuracy on the *NinaPro DB5* ($89.41 \pm 0.16\%$), *EPN-612* ($96.74 \pm 0.09\%$), and *UCI-EMG* ($97.56 \pm 0.32\%$) datasets. Furthermore, on the *Generic Neuromotor Interface – discrete-gesture* dataset, TinyMyo achieves a CLER of 0.153 ± 0.006 with an approximate 44% reduction in model size compared to the original work.

On the hand kinematic regression task, we achieve a MAE of 8.77 ± 0.12 with a subject-agnostic model. On the speech production task, we obtain a WER of $33.54 \pm 1.12\%$, which is comparable to the current SoA, while reducing the model size by approximately 91%. Finally, we demonstrate that TinyMyo can also adapt to the speech recognition task, achieving a WER of $33.95 \pm 0.97\%$.

TinyMyo is also the first FM for EMG deployed on the edge, achieving an inference in 12.2s at 0.44J, with an average power-envelope of 36.45mW.

We identify the following limitations, which will be addressed as part of future work:

- The datasets used for pre-training consist primarily of EMG recordings from the forearm and wrist during gesture-related tasks. Data from additional body locations (e.g., lower-limb muscle groups) should be included to improve anatomical generalization.
- Both the pre-training and downstream datasets were collected in controlled laboratory environments. Additional research is needed to evaluate the robustness of the proposed FM under realistic conditions, such as data corrupted by motion artifacts or environmental noise.
- Further studies are required to assess the model's generalization capabilities in zero-shot settings and to quantify

the amount of labeled data needed to achieve strong performance on novel downstream tasks.

- Despite demonstrating, to the best of our knowledge, the first deployment of an FM for EMG processing on an ultra-low-power microcontroller, the inference time remains too high for seamless use in real-world applications. Future work should therefore focus on optimizing the network architecture to minimize the computation needed for inference. This could be achieved by doing an ablation study on reducing the sequence length, by adopting a cheaper attention mechanism [32] or exploring more aggressive quantization techniques (e.g.: sub 8-bit [67]. More efficient architectures, such as state-space models (e.g., MAMBA [68], FEMBA [30]), whose computational cost scales linearly with the context length, would also be worth exploring. Moreover, distributing the computation over multiple GAP9 nodes or deploying it on more powerful platforms such as Siracusa [69] is expected to yield substantial speed-ups.

Architectural improvements and refinements in the training pipeline also represent an important future direction. We aim to explore alternative pooling mechanisms (e.g., attention-based) to weight per-channel contribution more precisely.

By open-sourcing¹ our pre-trained models and the architectures used for downstream evaluations, we aim to provide a versatile resource that can accelerate future research and serve as a foundation for the broader EMG community. Our intention is that other researchers will extend this backbone with additional datasets, improved training strategies, and architectural variations, aligning with the community-wide effort recently advocated by Eddy *et al.* [70].

ACKNOWLEDGMENT

The authors thank Chen Yanlong (ETH Zürich) for technical support and Lorenzo Lamberti (ETH Zürich) for fruitful discussions.

REFERENCES

- [1] D. Farina and R. M. Enoka, “Evolution of surface electromyography: From muscle electrophysiology towards neural recording and interfacing,” *Journal of Electromyography and Kinesiology*, vol. 71, p. 102796, 2023.
- [2] E. R. Avila, S. E. Williams, and C. Disselhorst-Klug, “Advances in emg measurement techniques, analysis procedures, and the impact of muscle mechanics on future requirements for the methodology,” *Journal of Biomechanics*, vol. 156, p. 111687, 2023. [Online]. Available: <https://www.sciencedirect.com/science/article/pii/S0021929023002567>
- [3] D. Xiong, D. Zhang, Y. Chu, Y. Zhao, and X. Zhao, “Intuitive human-robot-environment interaction with emg signals: A review,” *IEEE/CAA Journal of Automatica Sinica*, vol. 11, no. 5, pp. 1075–1091, 2024.
- [4] A. Cimolato, J. J. Driessens, L. S. Mattos, E. De Momi, M. Laffranchi, and L. De Michieli, “Emg-driven control in lower limb prostheses: A topic-based systematic review,” *Journal of NeuroEngineering and Rehabilitation*, vol. 19, no. 1, p. 43, 2022.
- [5] A. Marinelli, N. Boccardo, F. Tessari, D. Di Domenico, G. Caserta, M. Canepa, G. Gini, G. Barresi, M. Laffranchi, L. De Michieli *et al.*, “Active upper limb prostheses: A review on current state and upcoming breakthroughs,” *Progress in Biomedical Engineering*, vol. 5, no. 1, p. 012001, 2023.
- [6] P. Kaifosh, T. R. Reardon, and C. labs at Reality Labs, “A generic non-invasive neuromotor interface for human-computer interaction,” *Nature*, 2025. [Online]. Available: <https://www.nature.com/articles/s41586-025-09255-w>
- [7] M. Boyer, L. Bouyer, J.-S. Roy, and A. Campeau-Lecours, “Reducing noise, artifacts and interference in single-channel emg signals: A review,” *Sensors*, vol. 23, no. 6, 2023. [Online]. Available: <https://www.mdpi.com/1424-8220/23/6/2927>
- [8] R. Merletti and G. Cerone, “Tutorial. surface emg detection, conditioning and pre-processing: Best practices,” *Journal of Electromyography and Kinesiology*, vol. 54, p. 102440, 2020.
- [9] D. Xiong, D. Zhang, X. Zhao, and Y. Zhao, “Deep learning for emg-based human-machine interaction: A review,” *IEEE/CAA Journal of Automatica Sinica*, vol. 8, no. 3, pp. 512–533, 2021.
- [10] S. Ni, M. A. Al-qaness, A. Hawbani, D. Al-Alimi, M. Abd Elaziz, and A. A. Ewees, “A survey on hand gesture recognition based on surface electromyography: Fundamentals, methods, applications, challenges and future trends,” *Applied Soft Computing*, vol. 166, p. 112235, 2024.
- [11] X. Gu, Y. Shu, J. Han, Y. Liu, Z. Liu, J. Anibal, V. Sangha, E. Phillips, B. Segal, H. Yuan *et al.*, “Foundation models for biosignals: A survey,” *Authorea Preprints*, 2025.
- [12] S. Salter, R. Warren, C. Schlager, A. Spurr, S. Han, R. Bhasin, Y. Cai, P. Walkington, A. Bolarinwa, R. Wang, N. Danielson, J. Merel, E. Pnevmatikakis, and J. Marshall, “emg2pose: A Large and Diverse Benchmark for Surface Electromyographic Hand Pose Estimation,” Dec. 2024, arXiv:2412.02725 [cs]. [Online]. Available: <http://arxiv.org/abs/2412.02725>
- [13] Y. Chen, M. Orlandi, P. M. Rapa, S. Benatti, L. Benini, and Y. Li, “Physiowave: A multi-scale wavelet-transformer for physiological signal representation,” *arXiv preprint arXiv:2506.10351*, 2025.
- [14] —, “Waveformer: A lightweight transformer model for semg-based gesture recognition,” *arXiv preprint arXiv:2506.11168*, 2025.
- [15] S. Benatti, E. Donati, A. Moin, M. Zanghieri, M. Orlandi, A. Burrello, F. Artoni, S. Micera, L. Benini, and J. M. Rabaey, “Emg acquisition and processing for hand movement decoding on embedded systems: State of the art and challenges,” *Proceedings of the IEEE*, 2025.
- [16] S. Pizzolato, L. Tagliapietra, M. Cognolato, M. Reggiani, H. Müller, and M. Atzori, “Comparison of six electromyography acquisition setups on hand movement classification tasks,” *PLOS ONE*, vol. 12, no. 10, pp. 1–17, 10 2017. [Online]. Available: <https://doi.org/10.1371/journal.pone.0186132>
- [17] M. E. Benalcazar, L. Barona, L. Valdivieso, X. Aguas, and J. Zea, “EMG-EPN-612 Dataset,” Nov. 2020. [Online]. Available: <https://zenodo.org/records/4421500>
- [18] N. Krilova, I. Kastalskiy, V. Kazantsev, V. Makarov, and S. Lobov, “EMG Data for Gestures,” UCI Machine Learning Repository, 2018, DOI: <https://doi.org/10.24432/C5ZP5C>.
- [19] A. Krasoulis, S. Vijayakumar, and K. Nazarpour, “Effect of user practice on prosthetic finger control with an intuitive myoelectric decoder,” p. 891, 2019.
- [20] D. Gaddy and D. Klein, “Digital voicing of silent speech,” in *Proceedings of the 2020 Conference on Empirical Methods in Natural Language Processing (EMNLP)*, B. Webber, T. Cohn, Y. He, and Y. Liu, Eds. Online: Association for Computational Linguistics, Nov. 2020, pp. 5521–5530.
- [21] Ö. Turgut, P. Müller, M. J. Menten, and D. Rueckert, “Towards generalisable time series understanding across domains,” *arXiv preprint arXiv:2410.07299*, 2024.
- [22] F. Palermo, M. Cognolato, A. Gijsberts, H. Müller, B. Caputo, and M. Atzori, “Repeatability of grasp recognition for robotic hand prosthesis control based on semg data,” in *2017 International Conference on Rehabilitation Robotics (ICORR)*, 2017, pp. 1154–1159.
- [23] M. Goswami, K. Szafer, A. Choudhry, Y. Cai, S. Li, and A. Dubrawski, “Moment: A family of open time-series foundation models,” *arXiv preprint arXiv:2402.03885*, 2024.
- [24] W.-B. Jiang, X. Fu, Y. Ding, and C. Guan, “Towards robust multimodal physiological foundation models: Handling arbitrary missing modalities,” *arXiv preprint arXiv:2504.19596*, 2025.
- [25] W.-B. Jiang, L.-M. Zhao, and B.-L. Lu, “Large brain model for learning generic representations with tremendous eeg data in bci,” *arXiv preprint arXiv:2405.18765*, 2024.
- [26] D. Alvarez-Estevez and R. M. Rijssman, “Inter-database validation of a deep learning approach for automatic sleep scoring,” *PloS one*, vol. 16, no. 8, p. e0256111, 2021.
- [27] J. A. Brantley, T. P. Luu, S. Nakagome, F. Zhu, and J. L. Contreras-Vidal, “Full body mobile brain-body imaging data during unconstrained locomotion on stairs, ramps, and level ground,” *Scientific data*, vol. 5, no. 1, pp. 1–10, 2018.
- [28] Y. Nie, N. H. Nguyen, P. Sinthong, and J. Kalagnanam, “A time series is worth 64 words: Long-term forecasting with transformers,” in *The Eleventh International Conference on Learning Representations*.

¹after review

[29] Y. Bao, S. Sivanandan, and T. Karaletsos, "Channel vision transformers: An image is worth 1 x 16 x 16 words," *arXiv preprint arXiv:2309.16108*, 2024.

[30] A. Tegon, T. M. Ingolfsson, X. Wang, L. Benini, and Y. Li, "Femba: Efficient and scalable eeg analysis with a bidirectional mamba foundation model," *arXiv preprint arXiv:2502.06438*, 2025.

[31] B. Döner, T. M. Ingolfsson, L. Benini, and Y. Li, "LUNA: Efficient and topology-agnostic foundation model for EEG signal analysis," in *The Thirty-ninth Annual Conference on Neural Information Processing Systems*, 2025. [Online]. Available: <https://openreview.net/forum?id=uazfjnFL0G>

[32] A. Dimofte, G. A. Bucagu, T. M. Ingolfsson, X. Wang, A. Cossettini, L. Benini, and Y. Li, "Cerebro: Compact encoder for representations of brain oscillations using efficient alternating attention," *arXiv preprint arXiv:2501.10885*, 2025.

[33] J. Su, Y. Lu, S. Pan, A. Murtadha, B. Wen, and Y. Liu, "Roformer: Enhanced transformer with rotary position embedding," *arXiv preprint arXiv:2104.09864*, 2023.

[34] A. Vaswani, N. Shazeer, N. Parmar, J. Uszkoreit, L. Jones, A. N. Gomez, L. Kaiser, and I. Polosukhin, "Attention is all you need," *arXiv preprint arXiv:1706.03762*, 2023.

[35] R. Xiong, Y. Yang, D. He, K. Zheng, S. Zheng, C. Xing, H. Zhang, Y. Lan, L. Wang, and T.-Y. Liu, "On layer normalization in the transformer architecture," *arXiv preprint arXiv:2002.04745*, 2020.

[36] X. Liu, H. Peng, N. Zheng, Y. Yang, H. Hu, and Y. Yuan, "Efficientvit: Memory efficient vision transformer with cascaded group attention," *arXiv preprint arXiv:2305.07027*, 2023.

[37] G. Wang, W. Liu, Y. He, C. Xu, L. Ma, and H. Li, "Eegpt: Pretrained transformer for universal and reliable representation of eeg signals," *Advances in Neural Information Processing Systems*, vol. 37, pp. 39249–39280, 2024.

[38] Z. Xie, Z. Zhang, Y. Cao, Y. Lin, J. Bao, Z. Yao, Q. Dai, and H. Hu, "Simmim: A simple framework for masked image modeling," *arXiv preprint arXiv:2111.09886*, 2022.

[39] C. Zhang, C. Zhang, J. Song, J. S. K. Yi, K. Zhang, and I. S. Kweon, "A survey on masked autoencoder for self-supervised learning in vision and beyond," *arXiv preprint arXiv:2208.00173*, 2022.

[40] A. Krasoulis, I. Kyranou, M. Erden *et al.*, "Improved prosthetic hand control with concurrent use of myoelectric and inertial measurements," *Journal of NeuroEngineering and Rehabilitation*, vol. 14, p. 71, 2017.

[41] L. H. Smith, L. J. Hargrove, B. A. Lock, and T. A. Kuiken, "Determining the optimal window length for pattern recognition-based myoelectric control: Balancing the competing effects of classification error and controller delay," *IEEE Transactions on Neural Systems and Rehabilitation Engineering*, vol. 19, no. 2, pp. 186–192, 2011.

[42] C. De la Fuente, E. Martínez-Valdes, J. I. Priego-Quesada, A. Weinstein, O. Valencia, M. R. Kunzler, J. Alvarez-Ruf, and F. P. Carpes, "Understanding the effect of window length and overlap for assessing semg in dynamic fatiguing contractions: A non-linear dimensionality reduction and clustering," *Journal of Biomechanics*, vol. 125, p. 110598, 2021.

[43] J. Kaplan, S. McCandlish, T. Henighan, T. B. Brown, B. Chess, R. Child, S. Gray, A. Radford, J. Wu, and D. Amodei, "Scaling laws for neural language models," *arXiv preprint arXiv:2001.08361*, 2020.

[44] "A generic non-invasive neuromotor interface for human-computer interaction -GitHub Repository." [Online]. Available: <https://github.com/facebookresearch/generic-neuromotor-interface>

[45] A. Krasoulis, S. Vijayakumar, and K. Nazarpour, "Effect of user practice on prosthetic finger control with an intuitive myoelectric decoder," *Frontiers in neuroscience*, vol. 13, p. 891, 2019.

[46] D. Gaddy and D. Klein, "An improved model for voicing silent speech," *arXiv preprint arXiv:2106.01933*, 2021.

[47] "Voicing silent speech - github repository." [Online]. Available: https://github.com/dgaddy/silent_speech

[48] J. Kong, J. Kim, and J. Bae, "Hifi-gan: Generative adversarial networks for efficient and high fidelity speech synthesis," *arXiv preprint arXiv:2010.05646*, 2020.

[49] A. Baevski, H. Zhou, A. Mohamed, and M. Auli, "wav2vec 2.0: A framework for self-supervised learning of speech representations," *arXiv preprint arXiv:2006.11477*, 2020.

[50] M. Ravanelli, T. Parcollet, P. Plantinga, A. Rouhe, S. Cornell, L. Lugosch, C. Subakan, N. Dawalatabad, A. Heba, J. Zhong, J.-C. Chou, S.-L. Yeh, S.-W. Fu, C.-F. Liao, E. Rastorgueva, F. Grondin, W. Aris, H. Na, Y. Gao, R. D. Mori, and Y. Bengio, "SpeechBrain: A general-purpose speech toolkit," *arXiv preprint arXiv:2106.04624*, 2021.

[51] D. M. Gaddy, "Voicing silent speech," Ph.D. dissertation, University of California, Berkeley, 2022.

[52] A. Graves, S. Fernández, F. Gomez, and J. Schmidhuber, "Connectionist temporal classification: labelling unsegmented sequence data with recurrent neural networks," in *Proceedings of the 23rd international conference on Machine learning*, 2006, pp. 369–376.

[53] "LibriSpeech." [Online]. Available: https://docs.pytorch.org/audio/main/generated/torchaudio.models.decoder.download_pretrained_files.html

[54] P. Kenneweg, A. Schulz, S. Schröder, and B. Hammer, "Intelligent learning rate distribution to reduce catastrophic forgetting in transformers," in *Intelligent Data Engineering and Automated Learning – IDEAL 2022: 23rd International Conference, IDEAL 2022, Manchester, UK, November 24–26, 2022, Proceedings*. Berlin, Heidelberg: Springer-Verlag, 2022, p. 252–261. [Online]. Available: https://doi.org/10.1007/978-3-031-21753-1_25

[55] GreenWaves Technologies, "GAP SDK: Sdk for greenwaves technologies' gap8 iot application processor," https://github.com/GreenWaves-Technologies/gap_sdk, 2022, version 4.12.0.

[56] S. Kim, A. Gholami, Z. Yao, M. W. Mahoney, and K. Keutzer, "I-bert: Integer-only bert quantization," in *International conference on machine learning*. PMLR, 2021, pp. 5506–5518.

[57] M. Zanghieri, S. Benatti, A. Burrello, V. J. K. Morinigo, R. Meattini, G. Palli, C. Melchiorri, and L. Benini, "semg-based regression of hand kinematics with temporal convolutional networks on a low-power edge microcontroller," in *2021 IEEE International Conference on Omni-Layer Intelligent Systems (COINS)*. IEEE, 2021, pp. 1–6.

[58] M. Zanghieri, S. Benatti, L. Benini, and E. Donati, "Event-based low-power and low-latency regression method for hand kinematics from surface emg," 06 2023, pp. 293–298.

[59] T. Bao, Y. Zhao, S. A. R. Zaidi, S. Xie, P. Yang, and Z. Zhang, "A deep kalman filter network for hand kinematics estimation using semg," *Pattern Recognition Letters*, vol. 143, pp. 88–94, 2021. [Online]. Available: <https://www.sciencedirect.com/science/article/pii/S0167865521000118>

[60] Z. Ren, K. Scheck, Q. Hou, S. van Gogh, M. Wand, and T. Schultz, "Diff-ets: Learning a diffusion probabilistic model for electromyography-to-speech conversion," in *2024 46th Annual International Conference of the IEEE Engineering in Medicine and Biology Society (EMBC)*, 2024, pp. 1–4.

[61] K. Scheck and T. Schultz, "Multi-speaker speech synthesis from electromyographic signals by soft speech unit prediction," in *ICASSP 2023 - 2023 IEEE International Conference on Acoustics, Speech and Signal Processing (ICASSP)*, 2023, pp. 1–5.

[62] K. Scheck, T. Dombeck, Z. Ren, P. Wu, M. Wand, and T. Schultz, "Diffmv-ets: Diffusion-based multi-voice electromyography-to-speech conversion using speaker-independent speech training targets," *Interspeech 2025*, 2025. [Online]. Available: <https://api.semanticscholar.org/CorpusID:281892659>

[63] S. Sualiheen and D.-H. Kim, "Emgvox-gan: A transformative approach to emg-based speech synthesis, enhancing clarity, and efficiency via extensive dataset utilization," *Computer Speech & Language*, vol. 92, p. 101754, 2025. [Online]. Available: <https://www.sciencedirect.com/science/article/pii/S0885230824001360>

[64] J. Lee, Y. Oh, and K. Lee, "Speaking without sound: Multi-speaker silent speech voicing with facial inputs only," in *ICASSP 2025 - 2025 IEEE International Conference on Acoustics, Speech and Signal Processing (ICASSP)*, 2025, pp. 1–5.

[65] "wav2vec 2.0 with ctc trained on librispeech." [Online]. Available: <https://huggingface.co/speechbrain/asr-wav2vec2-librispeech>

[66] T. Benster, G. Wilson, R. Elisha, F. R. Willett, and S. Druckmann, "A cross-modal approach to silent speech with llm-enhanced recognition," *arXiv preprint arXiv:2403.05583*, 2024.

[67] P. Dong, L. Lu, C. Wu, C. Lyu, G. Yuan, H. Tang, and Y. Wang, "Packqvit: Faster sub-8-bit vision transformers via full and packed quantization on the mobile," *Advances in Neural Information Processing Systems*, vol. 36, pp. 9015–9028, 2023.

[68] A. Gu and T. Dao, "Mamba: Linear-time sequence modeling with selective state spaces," in *First conference on language modeling*, 2024.

[69] A. S. Prasad, M. Scherer, F. Conti, D. Rossi, A. Di Mauro, M. Eggimann, J. T. Gómez, Z. Li, S. S. Sarwar, Z. Wang *et al.*, "Siracusa: A 16 nm heterogenous risc-v soc for extended reality with at-mram neural engine," *IEEE Journal of Solid-State Circuits*, vol. 59, no. 7, pp. 2055–2069, 2024.

[70] E. Eddy, E. Campbell, C. Morrell, H. Williams, S. Bateman, and E. Scheme, "Raising the standard: an open source benchmarking platform and data repository to accelerate myoelectric control research," *Machine Learning: Health*, vol. 1, no. 1, p. 010601, 2025.